Geophysical Research Letters

RESEARCH LETTER
10.1029/2018GL080393

Stress Triggering of the 2005 Eruption of Sierra Negra Volcano, Galápagos

P. M. Gregg[1], H. Le Mével[2], Y. Zhan[1], J. Dufek[3], D. Geist[4,5], and W. W. Chadwick Jr.[6]

[1]Department of Geology, University of Illinois at Urbana-Champaign, Urbana, IL, USA, [2]Department of Terrestrial Magnetism, Carnegie Institution for Science, Washington, DC, USA, [3]Department of Earth Sciences, University of Oregon, Eugene, OR, USA, [4]Division of Earth Sciences, National Science Foundation, Alexandria, VA, USA, [5]Department of Geology, Colgate University, Hamilton, NY, USA, [6]NOAA Pacific Marine Environmental Laboratory, Hatfield Marine Science Center, Newport, OR, USA

Key Points:
- New thermomechanical models provide an estimation of magma system stability in the lead up to the 2005 eruption of Sierra Negra
- Models suggest that Sierra Negra's magma system was in stable storage prior to eruption with minimal overpressure and no tensile failure
- Coulomb static stress calculations indicate that a M_w 5.4 earthquake likely triggered the 2005 eruption

Supporting Information:
- Supporting Information S1

Correspondence to:
P. M. Gregg,
pgregg@illinois.edu

Citation:
Gregg, P. M., Le Mével, H., Zhan, Y., Dufek, J., Geist, D., & Chadwick, W. W., Jr. (2018). Stress triggering of the 2005 eruption of Sierra Negra volcano, Galápagos. *Geophysical Research Letters*, *45*. https://doi.org/10.1029/2018GL080393

Received 6 SEP 2018
Accepted 28 NOV 2018
Accepted article online 6 DEC 2018

Abstract Extensive vertical deformation (>4.5 m) observed at Sierra Negra volcano Galápagos, Ecuador, between 1992 and the 2005 eruption led scientists to hypothesize that repeated faulting events relieved magma chamber overpressure and prevented eruption. To better understand the catalyst of the 2005 eruption, thermomechanical models are used to track the stress state and stability of the magma storage system during the 1992–2005 inflation events. Numerical experiments indicate that the host rock surrounding the Sierra Negra reservoir remained in compression with minimal changes in overpressure (~10 MPa) leading up to the 2005 eruption. The lack of tensile failure and minimal overpressure accumulation likely inhibited dike initiation and accommodated the significant inflation without the need for pressure relief through shallow trapdoor faulting events. The models indicate that static stress transfer due to the M_w 5.4 earthquake 3 hr prior to the eruption most likely triggered tensile failure and catalyzed the 2005 eruption.

Plain Language Summary Tracking the stability of a magma system in the lead up to a volcanic eruption requires investigating both the pressure state of the magma reservoir and stress accumulation in the host rock. New coupled conduit flow-magma reservoir pressurization models are used to evaluate the evolution of the magma reservoir of Sierra Negra volcano, Galápagos, in the lead up to its 2005 eruption. Stress calculations indicate that the magma reservoir was stable prior to the 2005 eruption and that the eruption was likely triggered by a M_w 5.4 earthquake that occurred 3 hours prior to the event. The new modeling approach has important implications for tracking the stress evolution of magma systems to evaluate future unrest and eruption triggering mechanisms at volcanoes worldwide.

1. Introduction

A classic paradigm in volcanology is that eruption occurs when the pressure within a magma reservoir exceeds the strength of the host rock surrounding it (Fowler & Spera, 2008; Huppert & Woods, 2002; Jaupart & Vergniolle, 1989; Tait et al., 1989; Wilson, 1980). Referred to as "overpressure," magma chamber pressurization is often cited as the primary mechanism for triggering volcanic eruption. Overpressure is hypothesized to be generated by the rapid change in reservoir volume resulting from mechanisms such as the injection of new material, phase change, the exsolution of volatiles, or a combination of these processes (Blake, 1981; Stock et al., 2016). In this paradigm, eruption is generally preceded by the swelling of the ground surface as the magma chamber expands. Magma reservoir inflation and subsequent volcano deformation is observable using geodetic methods such as tiltmeters, Interferometric Synthetic Aperture Radar (InSAR), and Global Positioning System (GPS; Biggs & Pritchard, 2017; Bjornsson et al., 1977; Dvorak & Dzurisin, 1997; Dzurisin, 2000; Lu & Zhang, 2014; Massonnet & Sigmundsson, 2000; Segall, 2013; Sparks, 2003). Overpressure can be estimated from surface inflation using classic analytical models (e.g., McTigue, 1987; Mogi, 1958), providing a first-order assessment of the system's evolution. However, the links between surface deformation, magma chamber pressurization, and eruption potential remain elusive (Gregg et al., 2012, 2013; Masterlark, 2007). While overpressure facilitates magma evacuation, failure in the host rock surrounding a magma system, and in particular tensile failure at the magma-rock interface, is critical for catalyzing an eruption. As such, determining the stability of magma in storage by estimating host rock stress evolution is necessary for assessing eruption potential (Acocella, 2007, 2010; Gerbault et al., 2012; Gregg et al., 2012; Grosfils, 2007; Grosfils et al., 2015; Marti et al., 2008).

While the impact of stress change on eruption triggering has previously been recognized as important for assessing unrest and forecasting eruption potential (Chadwick et al., 2006; Manga & Brodsky, 2006; Sulpizio et al., 2017; Sulpizio & Massaro, 2017), overpressure is more often used when discussing the threshold for magma reservoir stability. In the case of the prolonged unrest and uplift period prior to the 2005 eruption of Sierra Negra Volcano in the Galápagos, trapdoor-faulting events were postulated to have relieved overpressure accumulation in the rapidly expanding magma reservoir (Amelung et al., 2000; Chadwick et al., 2006). Unfortunately, estimating the overpressurization of a magma body is challenging, especially when observations of unrest begin in the middle of an eruption cycle. It is exceedingly difficult to back out how much deformation has occurred prior to detailed geodetic measurements to determine the baseline pressure and stress state (Del Negro et al., 2009; Gregg et al., 2012; Masterlark, 2007; McTigue, 1987; Mogi, 1958). Recent fluid-structure finite element method modeling approaches provide a means for producing model predictions of magma chamber stability by tracking stress and strain in the host rock while calculating changes in overpressure associated with deformation (Gregg et al., 2015; Le Mével et al., 2016).

In this investigation, we take advantage of recent advancements in volcano, fluid-structure interaction modeling to calculate the stress evolution of the Sierra Negra magma system in the lead up to its 2005 eruption. Overpressure, Mohr-Coulomb failure, and tensile stress are estimated to determine the stability of the magma system as it evolves. Of particular focus in this investigation is the interplay between overpressure and stress accumulation in the host rock prior to the onset of eruption. Additionally, we investigate stress evolution due to the thermal effect of prolonged magma flux, thermal contraction, and crystallization and discuss distinguishing volume change due to crystallization and volatile exsolution from volume change due to magma injection.

2. Unrest and the 2005 Eruption of Sierra Negra

Sierra Negra is a 60 × 40-km basaltic shield volcano that comprises most of the southern portion of Isabela Island and is the largest of the Galápagos volcanoes (Figure 1; Reynolds & Geist, 1995). Significant data collection efforts preceded the 2005 eruption of Sierra Negra, including deformation observations from InSAR, campaign GPS (2001–2003), the installation of continuous GPS stations in 2002, and campaign microgravity studies conducted in 2001–2002, 2005, 2006, and 2007 (Amelung et al., 2000; Chadwick et al., 2006; Geist et al., 2006, 2008; Vigouroux et al., 2008). In the lead up to the 2005 eruption, Sierra Negra experienced two episodes of extraordinary uplift: ~38 cm/a from 1992 to 1999 and ~120 cm/a in 2004 to 2005 when it reached a rate of ~1 cm/day prior to the eruption. The observed preeruption inflation culminated in nearly 5 m of cumulative vertical displacement (Chadwick et al., 2006).

Analytical models of the 1992–1999 InSAR observations indicate a rapidly inflating sill located ~2.1 km beneath the Sierra Negra Caldera (Amelung et al., 2000). Significant uplift during this time period, $>$ 2 m, is thought to have triggered trapdoor faulting and a M_w 5.0 earthquake on 11 January 1998 (Amelung et al., 2000; Chadwick et al., 2006; Jonsson, 2009). From 2000 to 2002, deflation of 9 cm/a was observed and modeled as a contracting sill of similar depth and geometry as the inflation source modeled by Amelung et al. (2000; Geist et al., 2006). The subsidence might be attributed to degassing, magma withdrawal back into the plumbing system, and/or viscoelastic relaxation (Geist et al., 2006, 2008). In 2004, a new period of inflation commenced at a higher rate than observed in the 1990s (Chadwick et al., 2006) and with exponentially increasing rates (Figure 2a). At its peak, Sierra Negra experienced vertical uplift rates $>$1 cm/day, triggering additional moderate-sized earthquakes including a M_b 4.0 on 23 February 2005, a M_b 4.6 earthquake on 16 April 2005, and a M_w 5.4 earthquake ~3 hr prior to the 22 October 2005 eruption. The 2005 eruption initiated as a 13–14-km-high volcanic plume and included lava fountains originating from a 2-km-long fissure and continued focused lava fountains that fed lava flowing into the caldera (Geist et al., 2008). The eruption ceased on 30 October 2005 after ~8 days of activity.

3. Model Formulation, Results, and Discussion

Our numerical approach, described in detail in supporting information S1, utilizes previously developed and benchmarked, thermomechanical and fluid-structure interaction finite element method models (Anderson, 1936, 1951; de Silva & Gregg, 2014; Del Negro et al., 2009; Gregg et al., 2012, 2013; Grosfils, 2007; Hickey & Gottsmann, 2014; Le Mével et al., 2016; Smith et al., 2009). COMSOL Multiphysics 5.3a is used to calculate

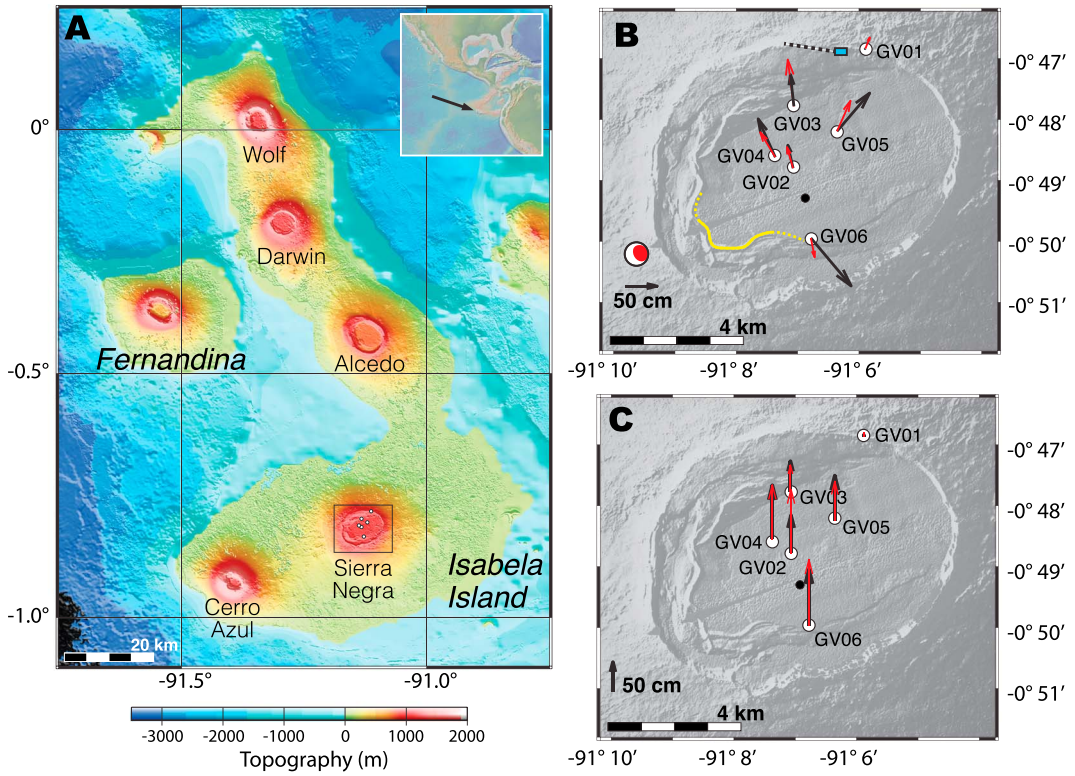

Figure 1. Best-fit thermomechanical model results compared to continuous GPS observations (Chadwick et al., 2006). (a) Location map. Data from GeoMapApp plotted with GMT. (b) Digital Elevation Model (DEM) of the summit of Sierra Negra (Yun et al., 2006) with the observed GPS horizontal displacements (black arrows) from 1 April 2003 to 21 October 2005 and modeled horizontal displacements (red arrows) for the entire time series. The center of the model source is depicted by the small black circle southeast of GV02. The precise location of the 22 October 2005 M_w 5.4 earthquake was not measured but is attributed to a fresh fault scarp (yellow and yellow dashed line) observed by Geist et al. (2008); the Global Central Moment Tensor (CMT) focal mechanism is provided (Dziewonski et al., 1981; Ekström et al., 2012). The initial eruption fissure is indicated by a black-dashed line on the north caldera scarp with the location of vents that remained active throughout the eruption depicted by a blue box. (c) The observed GPS vertical displacements (black arrows) from 1 April 2003 to 21 October 2005 and modeled vertical displacements (red arrows) for the entire time series from 1 April 2003 to 21 October 2005 (the misfit with GV02 reflects that the instrument went offline 10 June 2005, and GV01 was only operational until 3 December 2004). GPS = Global Positioning System.

the stress, strain, and temperature variations due to a viscous magma flowing from a deeper source into an existing, magma-filled reservoir (see supporting information S1 for full model details). A series of viscoelastic, fluid-structure interaction models was run to investigate the predicted stress evolution resulting from the observed surface deformation from 1992 to 2005. As the reservoir geometry and location (an ellipsoid 0.4 km tall × 7 km wide centered at 3-km depth) were constrained by previous geodetic studies (Amelung et al., 2000; Chadwick et al., 2006; Jonsson et al., 2005; Yun et al., 2006), we focus on the mass flux necessary to reproduce the uplift. Stability of the system is assessed by investigating the magnitude of the change in overpressure, the extent of Mohr-Coulomb failure in the host rock, and the presence of tensile failure along the magma reservoir boundary (Gregg et al., 2012, 2013, 2015; Grosfils, 2007; Grosfils et al., 2015). Overpressure is calculated as the local force per area along the reservoir-host rock interface with variable states of stress experienced for different regions of the interface. While the mere presence of significant pressurization, tensile failure, and/or through-going Mohr-Coulomb failure may not be sufficient to drive eruption, they provide a first-order approximation of stability. Although our discussions below focus on the fully coupled temperature-dependent viscoelastic calculations, a fully nontemperature-dependent, viscoelastic model (nTd1) and a model with nontemperature-dependent elastic moduli and a temperature-dependent viscosity (nTd2) are provided for comparison purposes (see Table S1 for model parameters and Table S2 for model variables). COMSOL's parameter sweep optimization was used to minimize the error between model predicted and observed vertical displacement.

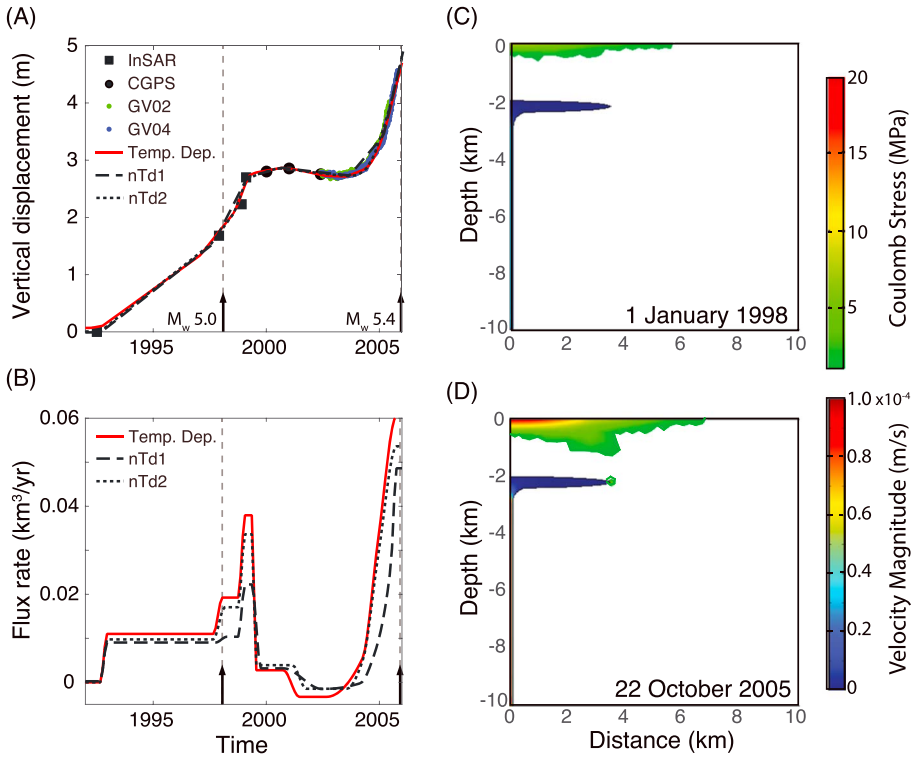

Figure 2. Model predicted flux variations leading up to the 2005 eruption. (a) Model predictions of vertical displacement from the best-fit temperature-dependent case (red solid line) and nontemperature-dependent models (black dashed and dotted lines) compared to InSAR (black squares), campaign Global Positioning System (black circles), and continuous Global Positioning System (colored circles) observations. (b) Flux boundary condition variations for the best-fit models. Data plotted from Chadwick et al. (2006). (c) Calculated Coulomb stress in the temperature-dependent model at 1 January 1998 just prior to the M_w 5.0 earthquake on 11 January 1998 (Amelung et al., 2000). White line is provided to highlight the 0-MPa Coulomb stress contour. (d) Calculated Coulomb stress in the temperature-dependent model on 22 October 2005 just prior to the recorded M_w 5.4 at 2034 UTC and eruption at 2330 UTC. Magma velocity magnitude is plotted within the reservoir and conduit. InSAR = Interferometric Synthetic Aperture Radar.

3.1. Preeruption Stress Evolution

The preeruption deformation of Sierra Negra is divided into three periods for model assessment: (1) the 1992–1999 inflation period; (2) the 2000–2003 deflation period; and (3) the preeruption 2004–2005 inflation period. To reproduce the 1992–1999 pattern of inflation, magma flux rates must average from 0.011 km^3/yr (Figure 2 and Tables S3–S5) through 1998 and increase to 0.03795 km^3/yr in 1998 (Figure 2b). In 1998, the best-fit model predicts Mohr-Coulomb failure and faulting in the upper 500 m of the model space (Figure 2c). The failure prediction coincides with the timing of observed seismicity including a M_w 5.0 earthquake on 11 January 1998 (Amelung et al., 2000). On the other hand, during the 1992–1999 inflation period, our models predict that the magma chamber should remain stable. There are no regions along the chamber boundary where tensile failure is observed and the predicted maximum change in reservoir overpressure remains modest (~6 MPa; Figure 3b and Table S4).

In 2000, there was deceleration and roll off in the uplift signal that is reproduced in the model by ceasing magma injection and allowing the host rock around the magma chamber to relax viscoelastically. However, reproducing the observed subsidence in 2001–2003 requires a decrease in the magma chamber volume. This can be achieved by allowing back flow of magma into the pipe at a rate of −0.0033 km^3/yr. Contraction due to conductive cooling during this time period does not produce an observable deformation signal due to its modest nature. In particular, the majority of the cooling occurs in a thin region along the flanks of the magma reservoir, while the central portion of the reservoir retains its temperature (within ~5 °C; Figure 3d). In response to the volume loss, the overpressure in the magma chamber is reduced by ~0.2 MPa (Figure 3b and Table S4). Similarly, tensile stress is reduced slightly, 0.2 MPa, along the chamber boundary

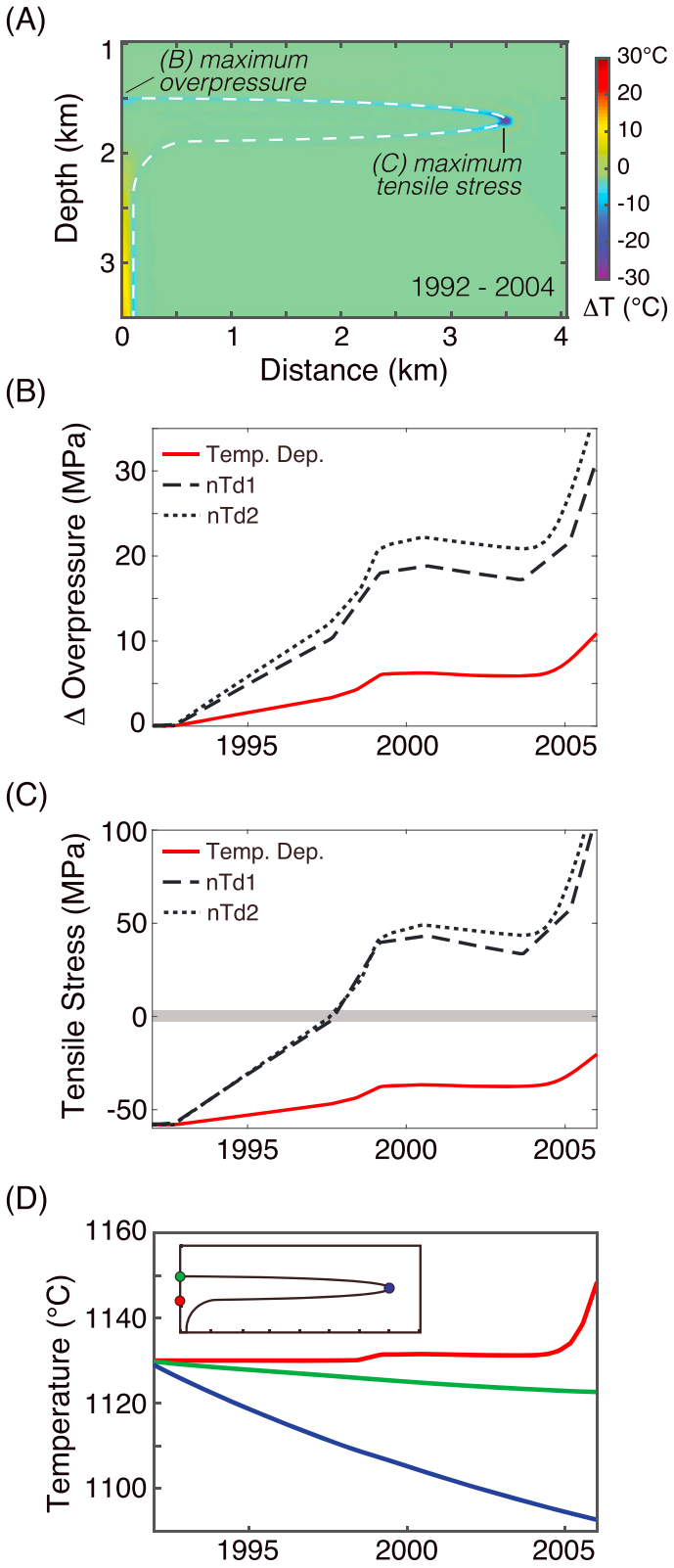

Figure 3. Model predictions of tensile stress and overpressure. (a) The change in model temperature observed from 1992 to 2005. The location of the maximum predicted tensile stress and maximum change in overpressure are indicated for (b) and (c). (b) Change in overpressure. (c) Maximum tensile stress. Negative tensile stress indicates compression, and positive tensile stress indicates tension. (d) Three points are investigated to compare the thermal evolution: above the central feeder conduit (red); the top, center of the reservoir (green); and the most distal point (blue).

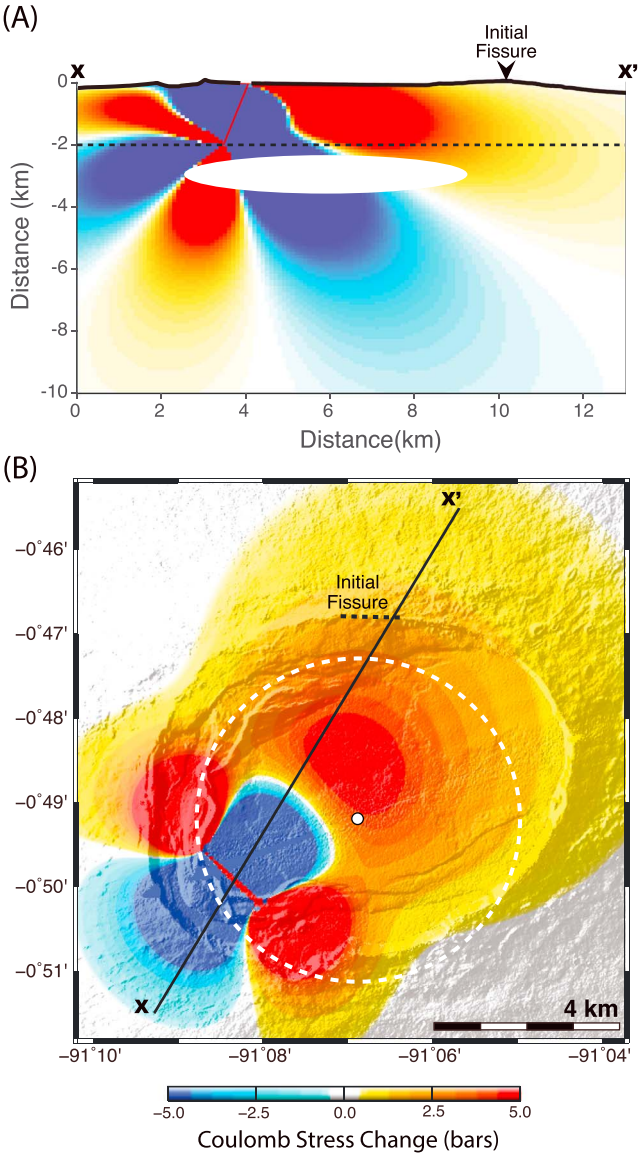

Figure 4. Calculated Coulomb static stress transfer on normal receiver faults due to the 22 October 2005 M_w 5.4 earthquake, which occurred 3 hr prior to Sierra Negra's eruption. Source parameters: seismic moment = 1.83e24 dyne * cm, strike = 146, dip = 74, Young's modulus = 50 GPa. (a) Cross section along X–X' indicated on (b) through the source fault and the location of the initial eruption fissure (block arrow). The red line indicates the location of the source fault, and the magma reservoir location is indicated by the white ellipse. Please note that the magma reservoir is not part of the Coulomb 3.4 calculation. The dashed line indicates the location of the map view stress plot. (b) A map view stress section draped over Sierra Negra topography (shaded relief) taken at 2-km depth showing the reservoir center (white circle) and greatest extent (white-dashed line).

(Figure 3c and Table S5). Overall, the time period of quiescence appears to be too brief and the rate of volume loss too modest to significantly impact the stress state of the magma system.

At the end of 2003, magma injection commences again at a higher rate of 0.033 km^3/yr. As the ground surface inflates, significantly larger regions of the shallow crust undergo Mohr-Coulomb failure. By 2005, the regions of the model space exhibiting Mohr-Coulomb failure is extensive, impacting the overlying roof down to ~1.5-km depth (Figure 2d). Tensile stress along the magma reservoir boundary also increases, but the entire reservoir boundary remains in a compressional regime (Figure 3c and Table S5). Overpressure also significantly increases reaching its highest point at the center of the reservoir of 10.7 MPa just prior to the 2005 eruption (Figure 4b and Table S4). However, at the time step prior to the 2005 eruption, the modeled reservoir remains have no tensile failure and only moderate overpressure suggesting that it should be stable. Nevertheless, the widespread nature of Mohr-Coulomb failure and potential for triggering seismicity raises important considerations for the role of earthquakes leading up to the 2005 eruption.

3.2. Earthquake Catalyst for the 2005 Eruption

In the lead up to the 2005 eruption, the models predict that the magma reservoir remains in a stable stress state with minimal overpressure and no tensile stress above 0 MPa on or near the reservoir boundary. Although a predicted magnitude of overpressure >10 MPa is generally cited as a minimum level for dike propagation (Rubin, 1995), the greatest overpressures are observed in the central portion of the magma chamber where compressive stresses are greatest and dike initiation is unlikely. Additionally, the eruption appears to have initiated from the flank of the magma system (Geist et al., 2008). However, while the magma system appears to be stable in the model, large regions of the host rock are predicted to be in Mohr-Coulomb failure in the time steps leading up to the 2005 eruption (Figure 3c). Moreover, 3 hr prior to the 22 October 2005 eruption, a M_w 5.4 earthquake occurred, likely rupturing along the sinuous ridge on the southwestern base of the caldera where ~150 cm of dip-slip was observed (Geist et al., 2008).

The Coulomb static stress transfer due to a M_w 5.4 earthquake is investigated utilizing the U.S. Geological Survey (USGS) Coulomb 3.4 software (Lin & Stein, 2004; Toda et al., 2005). As the exact rupture geometry is not constrained, we have chosen a central segment to represent the multisegment fault rupture (Figure 4b). Model results indicate that the 22 October 2005, 2034 UTC event likely relieved stress along the southwest portion of the caldera while increasing tensile stress, along the opposite, northeast region of the caldera and magma system (Figure 4). Three hours after the earthquake, the eruption initiated through a fissure on the north caldera rim. The triggering of volcanic events after has been previously observed (Chesley et al., 2012; Diez et al., 2005; Gregg et al., 2006; La Femina et al., 2004). Given the timing and location of the eruption, it is likely that the M_w 5.4 earthquake catalyzed the eruption on the opposite side of the magma reservoir where overpressure and tensile stresses were increasing but had not quite reached a critical threshold. Without the M_w 5.4 earthquake, the models predict that the magma reservoir would have continued to remain stable. The lack of eruption following the previous moderate earthquake events, M_w 5.0 on 11 January 1998 and M_b 4.6 on 16 April 2005, may indicate that the stress change due to the combination of reservoir inflation and the moderate-sized earthquake was not enough to trigger eruption.

An important caveat is that there is no deformation information prior to 1992 to constrain the stress state going into the inflation event. Two outcomes from the numerical experiments suggest that the approach is capturing some aspects of the preeruption stress evolution. First, the model-predicted increase in Coulomb failure (Figure 2c) is in agreement with the increase in seismicity and faulting observed at Sierra Negra in 1998 (e.g., Amelung et al., 2000). Were there to have been significant uplift prior to 1992, one would expect to see coincident seismicity, which is absent in the record. Second, the model indicates that the reservoir is priming for eruption but yet not failing in October 2008. Given the timing of the eruption, immediately following the M_w 5.4 earthquake, there is a strong suggestion that stress change induced by the earthquake pushed the reservoir, which was already primed, into eruption.

3.3. Thermal Impacts on Reservoir Stability

In long-lived magma systems with significant influx of heat and material, it is important to consider the thermal state of the host rock when assessing reservoir stability (Gregg et al., 2012, 2013; Jellinek & DePaolo, 2003). In the case of Sierra Negra, prolonged intrusion of material is likely to have increased the temperature of the host rock surrounding the reservoir, the effect of which is to lower both the viscosity and the elastic moduli of the host rock. The outcome of this reduction is to buffer stress accumulation, prevent failure, and increase stability (Gregg et al., 2012; Jellinek & DePaolo, 2003). By comparing the temperature-dependent model results to a nontemperature dependent, isoviscous (nTd1) case and a quasi-temperature-dependent case that includes constant elastic moduli but a temperature-dependent viscosity (nTd2), it appears that temperature plays a significant role in reducing the potential for failure when the impact on the elastic moduli is included. In the nTd model runs, the magma system is estimated to become unstable in 1998 after the first period of recorded inflation. At this time, the nTd models predict that the magma reservoir is in tensile failure and that the change in overpressure has surpassed 10 MPa. As the nTd models progress, both the tensile stress and change in overpressure are significant, reaching maximum values $>$30 and ~100 MPa, respectively. These values are likely untenable and indicate that models that do not include temperature-dependent elastic moduli are unable to provide a realistic estimation of the stress evolution of the Sierra Negra system given the lack of eruption until 2005.

3.4. Magma Injection Versus Volatile Exsolution

Microgravity observations led Vigouroux et al. (2008) to conclude that the rapid inflation period recorded in 2004–2005 leading up to the 2005 eruption may have been the result of second boiling (Blake, 1984; Tait et al., 1989) rather than the renewed injection of magma. The explosive nature of the opening phase of the 2005 eruption lends support to a volatile-driven pressure state. Furthermore, major element analysis using MELTS software indicates a 20 °C variation between the Early Phase and Main Phase erupted products of the 2005 event (1,128 to 1,108 °C, respectively), and ~13% crystallization is necessary to explain the trace element composition variation between the early and main phases (Geist et al., 2008). If the entire magma system were to have undergone such significant cooling and crystallization, crystallization-induced volatile exsolution is a very plausible eruption catalyst. As such, we investigate the extent of cooling during the 1992–2005 period of unrest.

When inflation paused between 1999 and 2003, the magma system should have experienced some cooling, but since information regarding the pre-1992 state of the magma system is unavailable, we cannot constrain whether the system had already undergone substantial cooling prior to the 1990s inflation event. The temperature-dependent model predicts a thin region of cooling, ~20°, at the flank of the reservoir between 1999 and 2003 but more modest cooling in the central portions of the reservoir near the conduit ($<$5°; Figure 3d). Although a volatile exsolution trigger cannot be fully ruled out, the subtlety and localized nature of the cooling observed in the model, which impacts only a small volume of the reservoir (Figure 3A), suggests that volatiles are an unlikely cause of the significant uplift observed prior to the 2005 eruption. Rather, a rejuvenation of magma injection is a more likely mechanism for the increased inflation in 2004–2005. Furthermore, the absence of crystals in the early phase of eruption (Geist et al., 2008) may indicate that the triggered dike that fed the initial eruption tapped a melt rich portion of the reservoir rather than a chilled and crystallized margin. An important caveat is that the true geometry and heterogeneity of the magma system may be more likened to an interconnected network of sills rather than a reservoir. Future efforts utilizing multiphase and perhaps 3-D modeling may be necessary to examine this problem in more detail.

Although magma compressibility is not included in the models, significant volatile content will impact the model results by increasing reservoir stability due to the inverse relationship between magma reservoir pressure and magma compressibility (see Section S1.1; e.g., Blake, 1981; Le Mével et al., 2016).

4. Conclusions

New numerical models focused on thermomechanical evolution indicate that the 2005 eruption of Sierra Negra volcano was likely triggered by a M_w 5.4 earthquake that preceded the event. Models of the stress evolution during the observed 18-year inflation event of >4.5 m of inflation suggest that Sierra Negra's magma system was in a stable storage configuration prior to its eruption in 2005 with ~11 MPa of accumulated overpressure and no indication of tensile failure along the reservoir boundary. However, the host rock accommodating the inflation had accumulated significant strain resulting in several earthquake/faulting events culminating in the M_w 5.4 earthquake, which triggered the eruption 3 hr later. Furthermore, estimates of temperature variation, which are modest and localized, suggest that a volatile overpressurization trigger is unlikely. The findings at Sierra Negra provide critical advancements for models of magma system stress state and system behavior in the lead up to eruptive events. This work has significant implications for the assessment of future unrest episodes, including the Sierra Negra's 2018 eruption, as well as forecasting magma system stability at other active volcanic systems.

Acknowledgments
The development of finite element modeling approaches for investigating magma chamber evolution and eruption is supported by grants from the National Science Foundation (OCE 1834843 and EAR 1752477—Gregg) and a NASA Earth and Space Science Fellowship (NASA 18-EARTH18F-0231—Zhan). Geist's effort is based upon work while serving at the National Science Foundation and was funded by NSF grant EAR-1145271. We are grateful for helpful discussions with J. Albright, H. Cabaniss, R. Goldman, V. Romano, and the UIUC Geodynamics Group. Model data in support of this manuscript are published in the PANGAEA data repository and available online (Gregg et al., 2018; https://doi.pangaea.de/10.1594/PANGAEA.896424). PMEL contribution number 4836.

References

Acocella, V. (2007). Understanding caldera structure and development; an overview of analog models compared to natural calderas. *Earth Science Reviews*, *85*, 125–160.

Acocella, V. (2010). Coupling volcanism and tectonics along divergent plate boundaries: Collapsed rifts from central Afar, Ethiopia. *Geological Society of America Bulletin*, *122*(9–10), 1717–1728. https://doi.org/10.1130/b30105.1

Amelung, F., Jonsson, S., Zebker, H., & Segall, P. (2000). Widespread uplift and 'trapdoor' faulting on Galapagos volcanoes observed with radar interferometry. *Nature*, *407*(6807), 993–996.

Anderson, E. M. (1936). The dynamics of the formation of cone sheets, ring dykes, and cauldron subsidence. *Royal Society of Edinburgh Proceedings*, *56*(2), 128–163.

Anderson, E. M. (1951). *The dynamics of faulting and dyke formation with applications in Britain* (2nd ed.). London: Oliver and Boyd.

Biggs, J., & Pritchard, M. E. (2017). Global volcano monitoring: What does it mean when volcanoes deform? *Elements*, *13*(1), 17–22. https://doi.org/10.2113/gselements.13.1.17

Bjornsson, A., Saemundsson, K., Einarsson, P., Tryggvason, E., & Gronvold, K. (1977). Current rifting episode in North Iceland. *Nature*, *266*(5600), 318–323. https://doi.org/10.1038/266318a0

Blake, S. (1981). Volcanism and the dynamics of open magma chambers. *Nature*, *289*, 783–785.

Blake, S. (1984). Volatile oversaturation during the evolution of silicic magma chambers as an eruption trigger. *Journal of Geophysical Research*, *89*(B10), 8237–8244. https://doi.org/10.1029/JB089iB10p08237

Chadwick, W. W. Jr., Geist, D. J., Jonsson, S., Poland, M., Johnson, D. J., & Meertens, C. M. (2006). A volcano bursting at the seams: Inflation, faulting, and eruption at sierra Negra volcano, Galapagos. *Geology*, *34*(12), 1025–1028. https://doi.org/10.1130/g22826a.1

Chesley, C., LaFemina, P. C., Puskas, C., & Kobayashi, D. (2012). The 1707 M_w8.7 Hoei earthquake triggered the largest historical eruption of Mt. Fuji. *Geophysical Research Letters*, *39*, L24309. https://doi.org/10.1029/2012gl053868

de Silva, S. L., & Gregg, P. M. (2014). Thermomechanical feedbacks in magmatic systems: Implications for growth, longevity, and evolution of large caldera-forming magma reservoirs and their supereruptions. *Journal of Volcanology and Geothermal Research*, *282*, 77–91. https://doi.org/10.1016/j.jvolgeores.2014.06.001

Del Negro, C., Currenti, G., & Scandura, D. (2009). Temperature-dependent viscoelastic modeling of ground deformation: Application to Etna volcano during the 1993-1997 inflation period. *Physics of the Earth and Planetary Interiors*, *172*, 299–309.

Diez, M., La Femina, P. C., Connor, C. B., Strauch, W., & Tenorio, V. (2005). Evidence for static stress changes triggering the 1999 eruption of Cerro Negro Volcano, Nicaragua and regional aftershock sequences. *Geophysical Research Letters*, *32*, L04309. https://doi.org/10.1029/2004gl021788

Dvorak, J. J., & Dzurisin, D. (1997). Volcano geodesy: The search for magma reservoirs and the formation of eruptive vents. *Reviews of Geophysics*, *35*(3), 343–384. https://doi.org/10.1029/97rg00070

Dziewonski, A. M., Chou, T.-A., & Woodhouse, J. H. (1981). Determination of earthquake source parameters from waveform data for studies of global and regional seismicity. *Journal of Geophysical Research*, *86*, 2825–2852. https://doi.org/10.1029/JB086iB04p02825

Dzurisin, D. (2000). Volcano geodesy: Challenges and opportunities for the 21st century. *Philosophical Transactions of the Royal Society of London, Series A: Mathematical, Physical and Engineering Sciences*, *358*(1770), 1547–1566. https://doi.org/10.1098/rsta.2000.0603

Ekström, G., Nettles, M., & Dziewonski, A. M. (2012). The global CMT project 2004-2010: Centroid-moment tensors for 13,017 earthquakes. *Physics of the Earth and Planetary Interiors*, *200-201*, 1–9. https://doi.org/10.1016/j.pepi.2012.04.002

Fowler, S. J., & Spera, F. J. (2008). Phase equilibria trigger for explosive volcanic eruptions. *Geophysical Research Letters*, *35*, L08309. https://doi.org/10.1029/2008gl033665

Geist, D., Chadwick, W., & Johnson, D. (2006). Results from new GPS and gravity monitoring networks at Fernandina and Sierra Negra Volcanoes, Galapagos, 2000-2002. *Journal of Volcanology and Geothermal Research*, *150*(1–3), 79–97. https://doi.org/10.1016/j.jvolgeores.2005.07.003

Geist, D. J., Harpp, K. S., Naumann, T. R., Poland, M., Chadwick, W. W., Hall, M., & Rader, E. (2008). The 2005 eruption of Sierra Negra volcano, Galapagos, Ecuador. *Bulletin of Volcanology*, *70*(6), 655–673. https://doi.org/10.1007/s00445-007-0160-3

Gerbault, M., Cappa, F., & Hassani, R. (2012). Elasto-plastic and hydromechanical models of failure around an infinitely long magma chamber. *Geochemistry, Geophysics, Geosystems*, *13*, Q03009. https://doi.org/10.1029/2011gc003917

Gregg, P. M., de Silva, S. L., & Grosfils, E. B. (2013). Thermomechanics of shallow magma chamber pressurization: Implications for the assessment of ground deformation data at active volcanoes. *Earth and Planetary Science Letters*, *384*, 100–108. https://doi.org/10.1016/j.epsl.2013.09.040

Gregg, P. M., de Silva, S. L., Grosfils, E. B., & Parmigiani, J. P. (2012). Catastrophic caldera-forming eruptions: Thermomechanics and implications for eruption triggering and maximum caldera dimensions on Earth. *Journal of Volcanology and Geothermal Research*, *241-242*, 1–12. https://doi.org/10.1016/j.jvolgeores.2012.06.009

Gregg, P. M., Grosfils, E. B., & de Silva, S. L. (2015). Catastrophic caldera-forming eruptions II: The subordinate role of magma buoyancy as an eruption trigger. *Journal of Volcanology and Geothermal Research*, *305*, 100–113. https://doi.org/10.1016/j.jvolgeores.2015.09.022

Gregg, P. M., Le Mével, H., Zhan, Y., Dufek, J., Geist, D., & Chadwick, W. W. (2018). COMSOL model data from Sierra Negra Volcano Galapagos Ecuador, 2005 eruption. *Pangea*. https://doi.org/10.1594/PANGAEA.896424

Gregg, P. M., Lin, J., & Smith, D. K. (2006). Segmentation of transform systems on the East Pacific Rise: Implications for earthquake processes at fast-slipping oceanic transform faults. *Geology*, *34*(4), 289–292.

Grosfils, E. B. (2007). Magma reservoir failure on the terrestrial planets: Assessing the importance of gravitational loading in simple elastic models. *Journal of Volcanology and Geothermal Research*, *166*(2), 47–75. https://doi.org/10.1016/j.jvolgeores.2007.06.007

Grosfils, E. B., McGovern, P. J., Gregg, P. M., Galgana, G. A., Hurwitz, D. M., Long, S. M., & Chestler, S. (2015). Elastic models of magma reservoir mechanics: A key tool for understanding planetary volcanism. In T. Platz, M. Massironi, P. Byrne, & H. Hiesinger (Eds.), *Volcanism and tectonism across the inner Solar System*, *Special Publications* (pp. 139–158). London: Geological Society. https://doi.org/10.1144/SP401.19

Hickey, J., & Gottsmann, J. (2014). Benchmarking and developing numerical finite element models of volcanic deformation. *Journal of Volcanology and Geothermal Research*, *280*, 126–130. https://doi.org/10.1016/j.jvolgeores.2014.05.011

Huppert, H. E., & Woods, A. W. (2002). The role of volatiles in magma chamber dynamics. *Nature*, *420*(6915), 493–495. https://doi.org/10.1038/nature01211

Jaupart, C., & Vergniolle, S. (1989). The generation and collapse of a foam layer at the roof of a basaltic magma chamber. *Journal of Fluid Mechanics*, *203*, 347–380. https://doi.org/10.1017/s0022112089001497

Jellinek, A. M., & DePaolo, D. J. (2003). A model for the origin of large silicic magma chambers: Precursors of caldera-forming eruptions. *Bulletin of Volcanology*, *65*(5), 363–381. https://doi.org/10.1007/s00445-003-0277-y

Jonsson, S. (2009). Stress interaction between magma accumulation and trapdoor faulting on Sierra Negra volcano, Galapagos. *Tectonophysics*, *471*(1–2), 36–44. https://doi.org/10.1016/j.tecto.2008.08.005

Jonsson, S., Zebker, H., & Amelung, F. (2005). On trapdoor faulting at Sierra Negra volcano, Galapagos. *Journal of Volcanology and Geothermal Research*, *144*(1–4), 59–71. https://doi.org/10.1016/j.jvolgeores.2004.11.029

La Femina, P. C., Connor, C. B., Hill, B. E., Strauch, W., & Saballos, J. A. (2004). Magma-tectonic interactions in Nicaragua: The 1999 seismic swarm and eruption of Cerro Negro volcano. *Journal of Volcanology and Geothermal Research*, *137*(1–3), 187–199. https://doi.org/10.1016/j.jvolgeores.2004.05.006

Le Mével, H., Gregg, P. M., & Feigl, K. L. (2016). Magma injection into a long-lived reservoir to explain geodetically measured uplift: Application to the 2007–2014 unrest episode at Laguna del Maule volcanic field, Chile. *Journal of Geophysical Research: Solid Earth*, *121*, 6092–6108. https://doi.org/10.1002/2016JB013066

Lin, J., & Stein, R. S. (2004). Stress triggering in thrust and subduction earthquakes and stress interaction between the southern San Andreas and nearby thrust and strike-slip faults. *Journal of Geophysical Research*, *109*, B02303. https://doi.org/10.1029/2003JB002607

Lu, Z., & Zhang, L. (2014). Frontiers of radar remote sensing. *Photogrammetric Engineering and Remote Sensing*, *80*(1), 5–13.

Manga, M., & Brodsky, E. (2006). Seismic triggering of eruptions in the far field: Volcanoes and geysers. *Annual Review of Earth and Planetary Sciences*, *34*, 263–291. https://doi.org/10.1146/annurev.earth.34.031405.125125

Marti, J., Geyer, A., Folch, A., & Gottsmann, J. (2008). A review on collapse caldera modelling. In J. Gottsmann & J. Marti (Eds.), *Caldera volcanism: Analysis, modelling and response* (pp. 233–283). Oxford, UK.

Massonnet, D., & Sigmundsson, F. (2000). Remote sensing of volcano deformation by radar interferometry from various satellites. In P. J. MouginisMark, J. A. Crisp, & J. H. Fink (Eds.), *Remote sensing of active volcanism* (pp. 207–221). Bath, UK.

Masterlark, T. (2007). Magma intrusion and deformation predictions: Sensitivities to the Mogi assumptions. *Journal of Geophysical Research*, *112*, B06419. https://doi.org/10.1029/2006JB004860

McTigue, D. F. (1987). Elastic stress and deformation near a finite spherical magma body: Resolution of a point source paradox. *Journal of Geophysical Research*, *92*, 15,977–15,990. https://doi.org/10.1029/JB092iB12p12931

Mogi, K. (1958). Relations of the eruptions of various volcanoes and the deformations of the ground surface around them. *Bulletin of the Earthquake Research Institute*, *36*, 99–134.

Reynolds, R. W., & Geist, D. J. (1995). Petrology of lavas from Sierra Negra volcano, Isabela Island, Galapagos archipelago. *Journal of Geophysical Research*, *100*(B12), 24,537–24,553. https://doi.org/10.1029/95JB02809

Rubin, A. M. (1995). Propagation of magma-filled cracks. *Annual Review of Earth and Planetary Sciences*, *23*, 287–336.

Segall, P. (2013). Volcano deformation and eruption forecasting. *Remote Sensing of Volcanoes and Volcanic Processes: Integrating Observation and Modelling*, *380*, 85–106. https://doi.org/10.1144/sp380.4

Smith, R., Sammonds, P. R., & Kilburn, C. R. J. (2009). Fracturing of volcanic systems: Experimental insights into pre-eruptive conditions. *Earth and Planetary Science Letters*, *280*, 211–219.

Sparks, R. S. J. (2003). Forecasting volcanic eruptions. *Earth and Planetary Science Letters*, *210*(1–2), 1–15. https://doi.org/10.1016/s0012-821x(03)00124-9

Stock, M. J., Humphreys, M. C. S., Smith, V. C., Isaia, R., & Pyle, D. M. (2016). Late-stage volatile saturation as a potential trigger for explosive volcanic eruptions. *Nature Geoscience*. https://doi.org/10.1038/NGEO2639

Sulpizio, R., Costa, A., & Wadge, G. (2017). Editorial: Stress field control of eruption dynamics. *Frontiers in Earth Science*, *5*(57). https://doi.org/10.3389/feart.2017.00057

Sulpizio, R., & Massaro, S. (2017). Influence of stress field changes on eruption initiation and dynamics: A review. *Frontiers in Earth Science*, *5*(18). https://doi.org/10.3389/feart.2017.00018

Tait, S., Jaupart, C., & Vergniolle, S. (1989). Pressure, gas content and eruption periodicity of a shallow, crystallizing magma chamber. *Earth and Planetary Science Letters*, *92*, 107–123.

Toda, S., Stein, R. S., Richards-Dinger, K., & Bozkurt, S. B. (2005). Forecasting the evolution of seismicity in southern California: Animations built on earthquake stress transfer. *Journal of Geophysical Research*, *110*, B05S16. https://doi.org/10.1029/2004JB003415

Vigouroux, N., Williams-Jones, G., Chadwick, W., Geist, D., Ruiz, A., & Johnson, D. (2008). 4D gravity changes associated with the 2005 eruption of Sierra Negra volcano, Galapagos. *Geophysics*, *73*(6), WA29–WA35. https://doi.org/10.1190/1.2987399

Wilson, L. (1980). Relationships between pressure, volatile content and ejecta velocity in 3 types of volcanic explosions. *Journal of Volcanology and Geothermal Research*, *8*(2–4), 297–313. https://doi.org/10.1016/0377-0273(80)90110-9

Yun, S., Segall, P., & Zebker, H. (2006). Constraints on magma chamber geometry at Sierra Negra Volcano, Galapagos Islands, based on InSAR observations. *Journal of Volcanology and Geothermal Research*, *150*(1–3), 232–243. https://doi.org/10.1016/j.jvolgeores.2005.07.009

Geophysical Research Letters

Supporting Information for

Stress Triggering of the 2005 eruption of Sierra Negra volcano, Galápagos

P. M. Gregg[1]*, H. Le Mével[2], Y. Zhan[1], J. Dufek[3], D. Geist[4,5], W. W. Chadwick Jr.[6]

[1] Department of Geology, University of Illinois, Urbana, IL, USA
[2] Department of Terrestrial Magnetism, Carnegie Institution for Science, Washington DC, USA
[3] Department of Earth Sciences, University of Oregon, Eugene, OR, USA
[4] Division of Earth Sciences, National Science Foundation, Alexandria, VA, USA
[5] Department of Geology, Colgate University, Hamilton, NY, USA
[5] NOAA Pacific Marine Environmental Laboratory, Hatfield Marine Science Center, Newport, OR, USA

Contents of this file

Introduction

Enclosed is the Supplementary methods summary, which includes model set up and numerical experiment implementation as well as tables of the parameters, variables, and model results.

S1. Methods

Our numerical approach utilizes previously developed and benchmarked, thermomechanical and fluid-structure interaction FEM models (Grosfils, 2007; Gregg *et al.*, 2012; Gregg *et al.*, 2013; Hickey and Gottsmann, 2014; Le Mével *et al.*, 2016). COMSOL Multiphysics 5.3a is used to calculate the stress, strain, and temperature variations due to a viscous magma flowing from a deeper source into an existing, magma-filled reservoir (Figure S1). A symmetry boundary is assumed on the left of the model, a free surface is assumed at the top of the model space, roller boundary conditions are applied on the right side and base of the model and an inlet boundary is assumed at the base of the conduit. Model parameters and variables are provided in Tables S1 and S2, respectively.

The presented COMSOL models utilized the following modules: Heat Transfer Module, LiveLink for MATLAB, Nonlinear Structural Materials Module, Structure Mechanics Module, and Subsurface Flow Module.

The geometry of the magma reservoir is determined from previous geodetic studies and is not varied in this modeling investigation (Amelung *et al.*, 2000; Jonsson *et al.*, 2005; Chadwick *et al.*, 2006; Yun *et al.*, 2006). An important note is that, while the system is being modeled as a reservoir being fed by a pipe, the geodetic observations do not provide constraints on the lower geometry of the reservoir or the feeding system into the reservoir. As Yun *et al.* (2006) illustrated nicely, a diapiric model setup is indistinguishable from a pressurized ellipsoid.

The sill-like geometry we have chosen (Amelung *et al.*, 2000; Jonsson *et al.*, 2005; Chadwick *et al.*, 2006) is also the geometry most susceptible to failure and eruption. In particular, previous modeling investigations (e.g., Gregg et al., 2013) have shown that as the aspect ratio of the ellipsoid (horizontal radius, *a*, / vertical radius, *b*) increases, the stability of the reservoir increases. This increase in stability is due to two effects. First, as the ellipsoid becomes more spherical and less oblate, tensile stress is reduced along the vertex of the ellipsoid. Second, larger reservoirs require lower changes in overpressure to produce the same magnitude of surface deformation as smaller reservoirs. See Supplemental Section S1.6 for additional information.

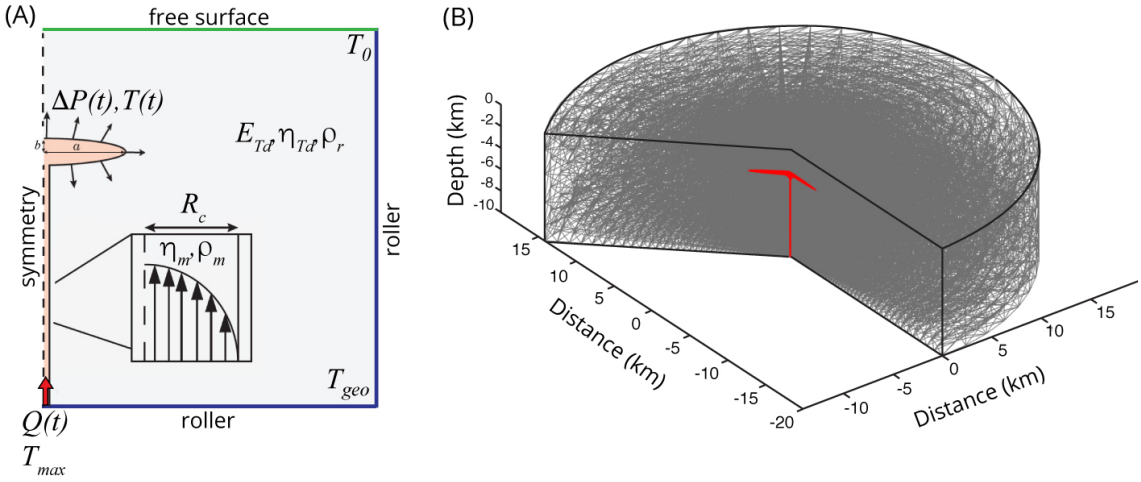

Figure S1. Fluid-structure interaction model setup after Le Mével *et al.* (2016). (A) The model setup includes a conduit through which magma is transported from a deep source (>10 km) into an existing shallow reservoir. The model is 2D axisymmetric with roller boundary conditions on the side and bottom and a free boundary at the surface. The magma reservoir expands due to the injection of magma from below. The wall rock is assumed to be a viscoelastic medium with temperature-dependent viscosity and elastic moduli. (B) The model mesh for the Sierra Negra implementation has a very dense mesh near the reservoir-rock interface with a coarse mesh at the edge of the model space.

S1.1 Fluid-structure interaction model

The host rock surrounding the magma reservoir is treated as a linear Maxwell viscoelastic solid:

$$\frac{d\varepsilon}{dt} = \frac{\sigma}{\eta} + \frac{1}{G}\frac{d\sigma}{dt} \qquad (1)$$

where ε is strain, and σ is stress. The total shear modulus, G, is a function of the Young's modulus, E: $G=E/2(1+\upsilon)$, where υ is Poisson's ratio.

Three suites of numerical experiments are run: (1) non-temperature dependent, isoviscous model that assumes constant elastic moduli and viscosity (nTd1); (2) a model that assumes constant elastic moduli, but a temperature dependent viscosity (nTd2); and (3) a fully temperature-dependent model that assumes temperature dependent values for the viscosity and elastic moduli (Temp. Dep., Td). See Section S1.1 for the thermal modeling approach.

The magma is treated as a single phase, incompressible, Newtonian fluid with a dynamic viscosity η_m and density ρ_m. In nature, magma is a three-phase mixture of melt, crystals, and melt, as such the chosen parameters represent the bulk material properties of a mafic magma (Geist *et al.*, 2008; Le Mével *et al.*, 2016). The governing equations for the conservation of mass and momentum are:

$$\nabla \cdot \mathbf{u} = 0\,, \tag{2}$$

and

$$\rho\left(\frac{\partial u}{\partial t} + u \cdot \nabla u\right) = -\nabla p + \eta_{eff}\nabla^2 u\,, \tag{3}$$

respectively, where ρ is the density of the mantle, p is pressure, **u** is velocity field, η_{eff} is the effective magma viscosity, C_p is the heat capacity, T is temperature, and k is thermal conductivity. The governing Navier-Stokes equation for fluid flow and viscoelastic equations are solved simultaneously using COMSOL's MUMPS solver. The COMSOL Multiphysics approach has been benchmarked with the analytical solutions for fluid-structure interaction by Le Mével *et al.* (2016).

Previous modeling investigations by Le Mével *et al.* (2016) illustrate the sensitivity of this approach to magma compressibility. Magma compressibility is inversely related to overpressure through its inverse relationship with bulk modulus, K. In particular, change in magma reservoir pressure:

$$\Delta P = K\frac{\Delta V}{V_0}\,, \tag{4}$$

where ΔV is the change in magma reservoir volume and V_0 is the initial reservoir volume. The bulk modulus is related to the inverse of the compressibility of the magma (β_m) and the compressibility host rock (β_r):

$$K = \frac{1}{\left(\beta_m + \beta_r\right)}\,, \tag{5}$$

such that

$$\Delta P = \frac{\Delta V}{V_0\left(\beta_m + \beta_r\right)}\,. \tag{6}$$

Increasing Magma compressibility impacts the model results in three important ways: (1) increasing the predicted magma flux; (2) reducing the predicted change in overpressure; and (3) reducing the predicted accumulation of tensile stress along the magma chamber boundary. Reduction in magma compressibility does not impact predictions of Mohr-Coulomb failure, which are most sensitive to the elastic moduli used to describe the host rock. Effectively, increasing magma compressibility allows the magma system to accommodate greater mass flux. We present models with incompressible magma, but note that increasing magma compressibility will act to further stabilize the magma system.

S1.2 Thermal model

The thermal structure is solved in COMSOL 5.3a using a two-step implementation. In the first step, a steady state thermal structure is calculated to provide the initial temperature at time, t = 0 (Figure S2A), for the second step, which is the time dependent thermal structure calculation.

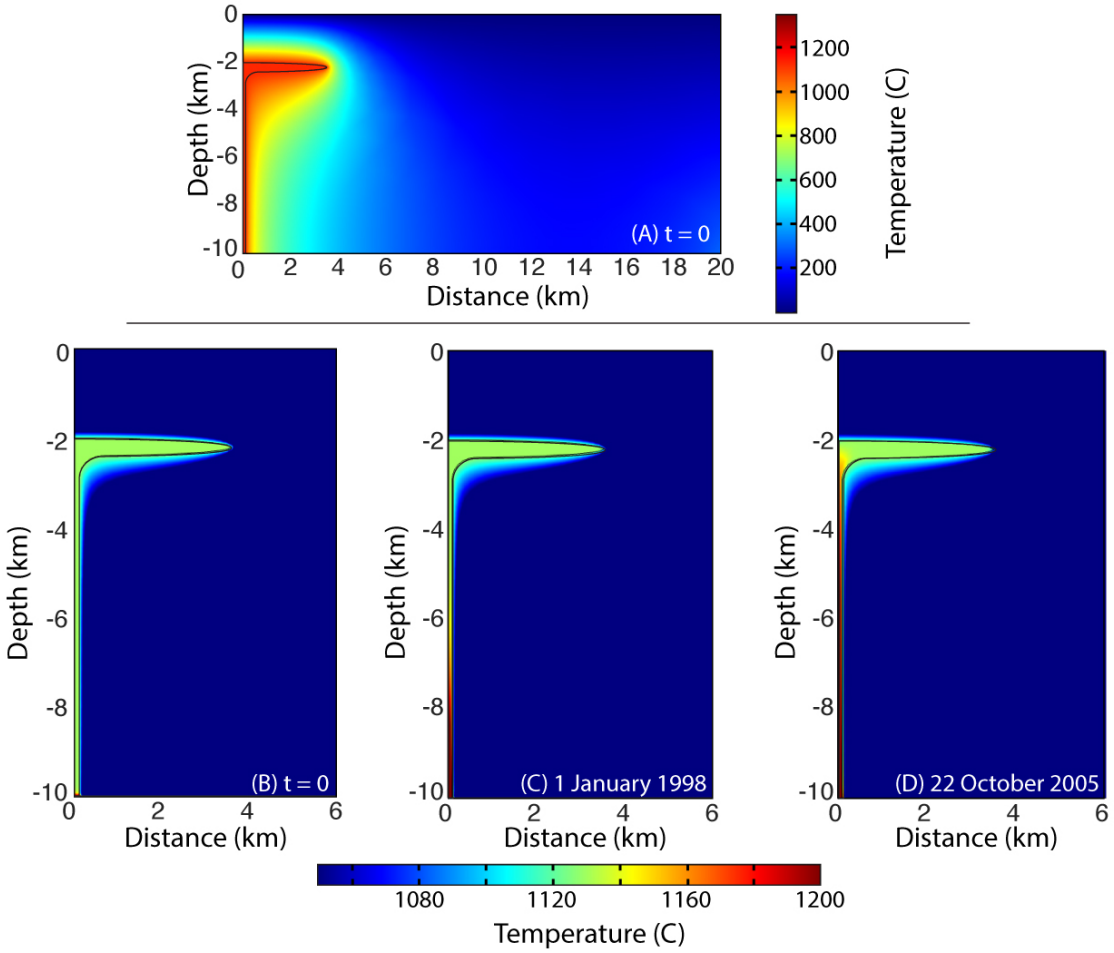

Figure S2. The thermal evolution of the model space. (A) Time, t = 0, is solved for using a steady state thermal calculation. (B) – (D) As time advances, the effect of injecting warmer magma into the shallow reservoir is tracked as well as the impact on heating the surrounding host rock. Because the temperature change is so small during this time period, the scale has been reduced. Figure 4 in the main text provides an overall change in temperature and evolution for three points in the model space.

The initial thermal structure for time = 0 is solved numerically from the steady-state heat conduction equation:

$$\nabla \cdot \left(k \nabla T \right) = -Q, \tag{7}$$

where k is the thermal conductivity, T is temperature, and Q is the crustal volumetric heat production, assumed to be zero. An initial magma temperature is of 1130°C is assumed in the reservoir and conduit. An initial background geotherm of 30°C/km is assumed. Although volcanic systems are transient and unlikely to reach a steady state thermal equilibrium, this provides an end-member starting point. The non-temperature dependent, isoviscous models are provided for comparison.

The time-dependent thermal model assumes a 1200°C deep source (> 10 km depth), which fluxes magma into a 200 m radius conduit that intrudes a 1130°C shallow source at 2.5 km depth (Figure 1). In this implementation, there is input of heat into the shallow magma reservoir through time as well as conductive heat loss across the magma reservoir-host rock interface. The thermal evolution of the magma is solved numerically by solving the governing equation for conservation of energy:

$$\rho C_p \mathbf{u} \cdot \nabla T + k \nabla^2 T = 0 , \quad (8)$$

where C_p is the heat capacity, T is temperature, and k is thermal conductivity (Figure 2B-D). COMSOL solves for the time-dependent thermal structure simultaneously with the fluid flow and solid mechanics calculations outlined above. The multiphysics approach allows for a self-consistent temperature-dependent model formulation in which the temperature-dependent viscosity and elastic moduli are updated at each time step (Figure S3).

The temperature-dependent viscosity of the host rock is calculated using the Arrhenius formulation:

$$\eta_{Td} = A_D \exp\left(\frac{E_A}{R_g T}\right), \quad (9)$$

where A_D is the Dorn parameter, E_A is the activation energy, and R_g is the universal gas constant (Del Negro *et al.*, 2009; Gregg *et al.*, 2012; de Silva and Gregg, 2014) .

Temperature and pressure also impact the elastic properties of the host rock and the resultant model predictions (Smith *et al.*, 2009; Gregg *et al.*, 2012; Gregg *et al.*, 2013). As such, we have incorporated a temperature and depth-dependent Young's modulus:

$$E_{Td} = E_m + \frac{E_0}{1 + C1 \exp\left(C2\left(1 - \frac{T}{T_{\max}}\right)\right)}, \quad (10)$$

where E_m is the minimum Young's modulus, E_0 is the initial Young's modulus, T_{max} is the maximum temperature (Figure S3B). Equation 10 provides a smooth transition between E_m and E_0 to minimize computational issues and mimic nature, which likely has a transition rather than sharp boundary in material properties.

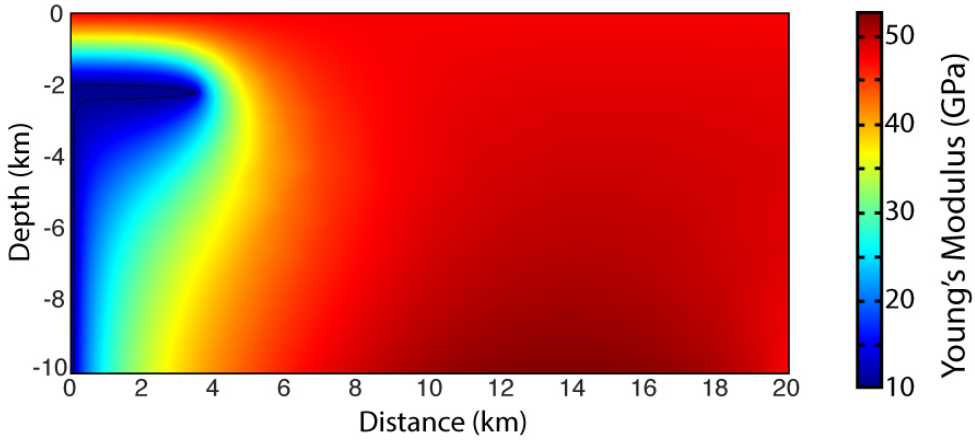

Figure S3. Temperature and depth-dependent Young's modulus at t = 0.

S1.3 Failure estimation

Failure in the host rock surrounding a reservoir is critically important for determining the stability of the system and potential for eruption (Anderson, 1936; 1951; Acocella, 2007; Marti *et al.*, 2008; Acocella, 2010; Gerbault *et al.*, 2012; Gregg *et al.*, 2012; Grosfils *et al.*, 2015). We use a combination of two approaches to predict magma chamber stability. First, we investigate faulting and failure in the brittle portions of the model space using a Mohr-Coulomb failure criterion:

$$\tau = C + f\sigma_n \tag{11}$$

where τ is the shear stress at failure, C is cohesion, f is the internal friction coefficient, and σ_n is the mean stress normal to the failure plane. Second, we investigate the evolution of tensile stresses, $\sigma_{ts,}$ which are defined as the least compressive stress along the magma chamber boundary. In application, as a magma system grows and inflates, the expansion results in flexure and uplift of the overlying roof, promoting faulting and brittle failure. Simultaneously, tensile stresses along the chamber boundary can result in Mode-I failure and dike initiation (Grosfils, 2007; Gregg *et al.*, 2012; Grosfils *et al.*, 2015).

S1.4 Overpressure Evolution

The main text of the paper focuses on the maximum change in overpressure predicted at the top of the magma reservoir by three rheological model implentations: temperature-dependent (Td), non-temperature dependent with constant elastic moduli and constant viscosity (nTd1), and non-temperature dependent with constant elastic moduli and a temperature-dependent viscosity (nTd2). In all of the models, the buoyancy of the magma, which is inherent in the slight density contrast, results in focusing of material towards the center of the reservoir. This magma focusing produces the greatest increases in overpressure at the reservoir's center or top. However, as the 2005 eruption was triggered from the flank of the reservoir, the pressure evolution predicted at the side of the reservoir is also of interest.

As there is no way to know the pressure condition at the start of the deformation time series, there is no way to back out the final overpressure prior to the 2005 eruption. However, it is likely that the modest reduction in overpressure predicted by the Td model (~9 MPa) was not enough to prevent eruption from catalyzing.

One aspect to the nTd models is that they result in much greater variations in predictions of overpressure – both in the maximum observed at the top of the reservoir and the minimum observed at the side. The temperature-dependent elastic moduli act to buffer both increases and decreases in overpressure. Effectively, models that do not incorporate the dependency of elastic moduli result in a drastic decrease in overpressure along the side of the reservoir. Given the explosive start of the eruption, it is unlikely that a pressure drop of ~100 MPa is reasonable.

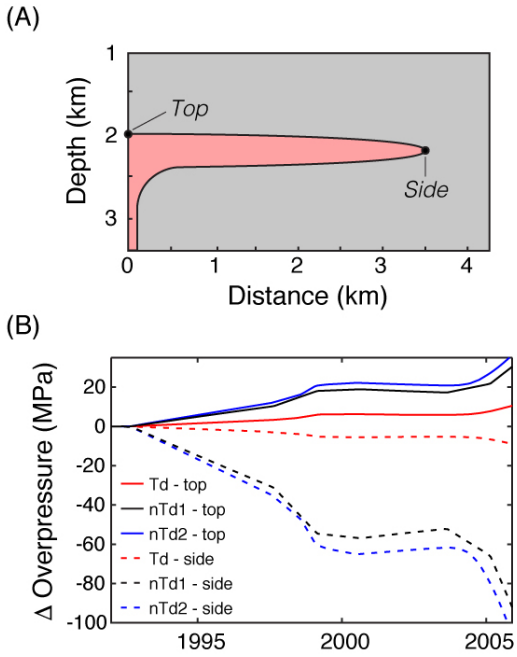

Figure S4. The change in reservoir boundary overpressure in time. (A) For illustrative purposes, points at the top of the magma reservoir and the side of the magma reservoir are chosen where the change in overpressure is at its maximum and minimum, respectively. (B) The rheology of the model has a strong impact on how pressure is accommodated due to the injection of magma into the reservoir. We investigate the fully temperature-dependent model (Td), a model with no temperature dependence in either the viscosity or the elastic moduli (nTd1), and a model with a temperature-dependent viscosity, but constant elastic moduli (nTd2). The buoyancy of the magma causes it to focus towards the center of the reservoir and away from the flanks. This process results in a decrease in overpressure at the flanks of the reservoir which is most pronounced in the non-temperature dependent cases. The temperature dependent case results in a slight reduction in pressure (~9 MPa). It is important to note that the initial pressure state of the magma reservoir is unknown and is unlikely to be 0 MPa.

S1.5 Coulomb static stress transfer

To investigate the static stress change resulting from the 22 October 2005 M_w 5.4 earthquake we utilize the USGS Coulomb 3.4 Coulomb static stress software (Lin and Stein, 2004; Toda *et al.*, 2005). The Coulomb stress change is defined as:

$$\Delta CFF = \Delta\tau + \mu_f \Delta\sigma_n, \quad (12)$$

where $\Delta\tau$ is the change in shear stress (positive in the slip direction), μ_f is the apparent friction coefficient, and $\Delta\sigma_n$ is the change in normal stress (positive indicates unclamping).

The fault plane solution for the 22 October 2005 earthquake is provided by the Global Central Moment Tensor (CMT) Catalog (Dziewonski *et al.*, 1981; Ekström *et al.*, 2012). The Scalar Moment was estimated at 1.83e24 dyne cm, with a strike of 148°, dip of 74°. As the location is not well constrained by the CMT Catalog, we assume the earthquake ruptured along the southwestern ring fracture where ~150 cm of dip-slip was observed (Geist *et al.*, 2008). As Coulomb 3.4 does not calculate stress transfer for complex or curved geometries, we assume a linear fault trace, 1.5 km long that ruptured to 2 km depth (Figure 6 of the main text).

S1.6 Geometrical considerations

A sill-like geometry was chosen in agreement with previous geodetic investigations (Amelung *et al.*, 2000; Jonsson *et al.*, 2005; Chadwick *et al.*, 2006). As previous numerical experiments have illustrated, the aspect ratio of the magma chamber may impact its stability and propensity towards rupture (Gregg *et al.*, 2013). To investigate whether the thickness of the assumed Sierra Negra magma reservoir will greatly affect the model results, we provide three additional models where the half height is 50 m, 75 m, and 100 m to compare to the 200 m model shown in the main text (Figures S5, S6, and S7). Note that the flux needed to reproduce the surface deformation does not vary between these models and the R1 = 200 m presented in the main text.

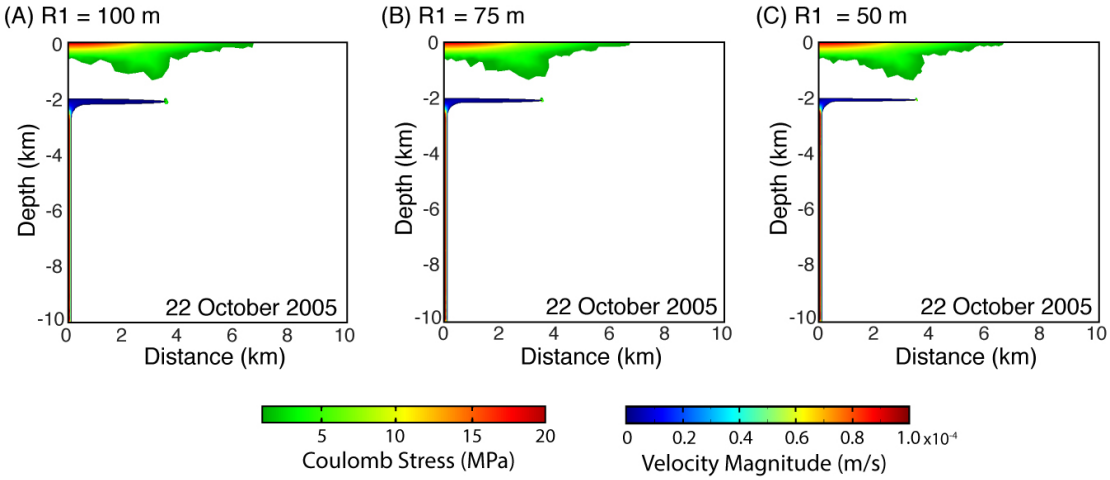

Figure S5. Calculated Coulomb stress for three additional model geometry half heights: (A) R1 = 100 m; (B) R1 = 75 m; and (C) R1 = 50 m. Coulomb stress is illustrated in the host rock and the flux velocity is shown in the magma reservoir and conduit.

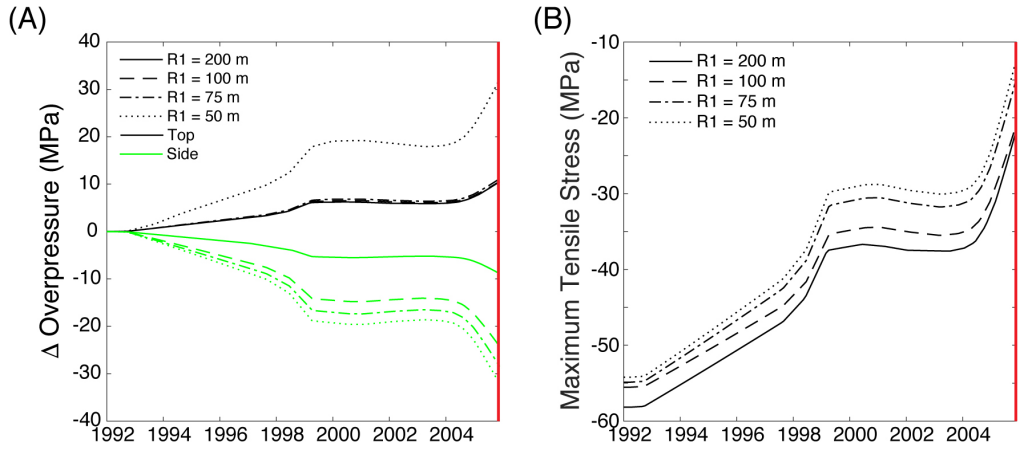

Figure S6. (A) Calculated change in overpressure at the top and side of the magma chamber (black and green respectively, see Figure S4A) for the three half heights. There is a significant jump in the predicted overpressure for R1 = 50 m. (B) Calculated maximum tensile stress along the magma chamber boundary for the three half heights. All of the configurations remain in compression for the entire time series leading up to the eruption (red vertical line).

While the extent of the predicted Coulomb failure does not vary significantly, an important outcome of this test is that at sill with a 50 m half-height exhibits a significant jump in the predicted overpressure as compared to the 200 m model (Figure S6A). However, all of the model geometries remain in compression with no tensile failure in the lead up to the final time step of the eruption. We speculate that even with the increase in the change in overpressure, tensile failure along the magma chamber boundary is necessary for dike initiation to produce an eruption. As such, a catalyst, such as the M_w 5.4 earthquake that occurred 3 hours prior to the eruption, may be necessary to push the reservoir into tensile failure.

S1.7 RMSE estimations for the model runs

COMSOL's optimization parameter sweep was utilized to find the best-fit flux rate for the forward models. The starting geometry was held constant between the different model implementations except for the models illustrated in Supplemental Section S1.6.

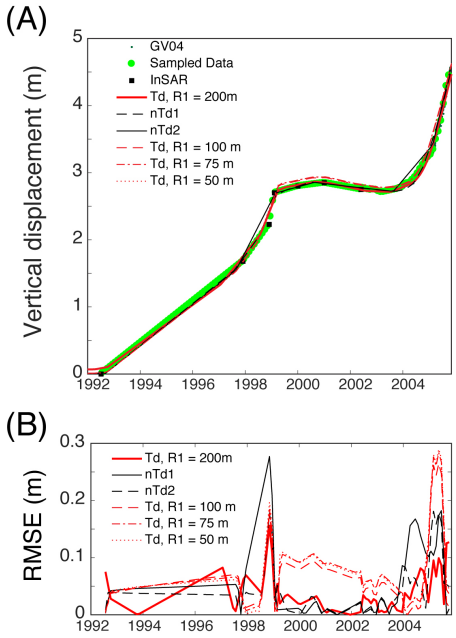

Figure S7. (A) Comparison of the vertical deformation predicted by the models and observed by the InSAR and GPS data. The data have been resampled at regular interval for model-data comparison (green circles). (B) Root mean square error (RMSE) for each of the model runs. The main misfit occurs when the deformation signal accelerates in 1998 and 2004.

S1.8 Pre-existing weakness

The surface expression of the Sierra Negra caldera is marked by an active sinuous ridge fault that may play a role in the evolution and stability of the Sierra Negra magma system (Amelung *et al.*, 2000; Chadwick *et al.*, 2006). Because the models assume a pristine host rock with no pre-existing weaknesses, we have run a test to investigate the effect of a shallow weak zone associated with caldera faults. The weak zone is implemented as a 90% reduction in elastic moduli coinciding with a 20 m wide fault zone located 3 km from the center of deformation, outward dipping at 74° to 1 km depth. The fault dip and location are chosen to coincide with the fault plane solution and estimated location of the 22 October 2005 M_w 5.4 earthquake

(Dziewonski *et al.*, 1981; Geist *et al.*, 2008; Ekström *et al.*, 2012). The addition of the fault does not result in a significant decrease in the maximum overpressure generated within the magma reservoir (Table S4). Because the region of greatest overpressure is located in the central portion of the magma reservoir 3 km away from the fault location, the flanking fault does not appear to provide a means for overpressure relief. Additionally, the inclusion of a caldera fault results in only a modest change in the maximum tensile stress, which is ~0.15 MPa more than the pristine temperature dependent model in 2001-2004 and ~0.65 MPa less at the time step prior to the 2005 eruption (Table S5). The extent of Mohr-Coulomb failure is slightly reduced by the inclusion of the fault, but is not significantly impacted (Figure S10C and S10D).

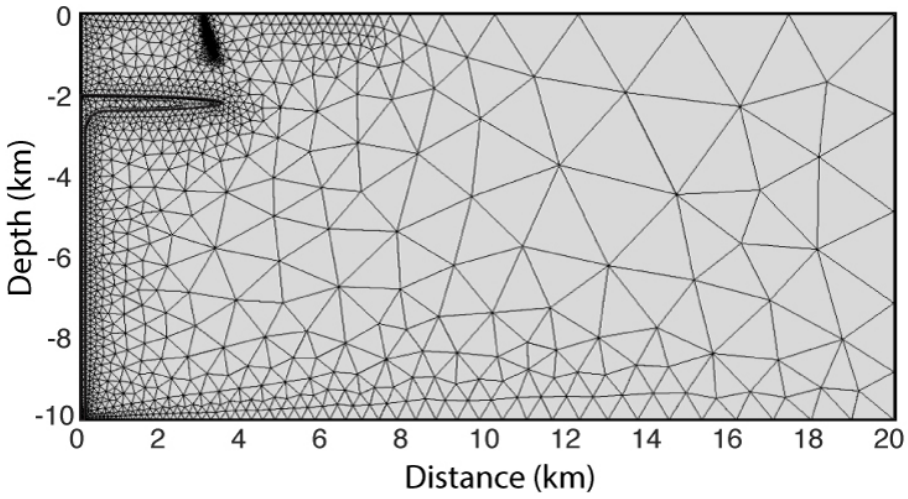

Figure S8. Pre-existing weakness implementation mesh. A 20 m wide fault is assumed 3 km from the center of the model dipping 74° down to 1 km. In this region the Young's modulus is decreased by 90%.

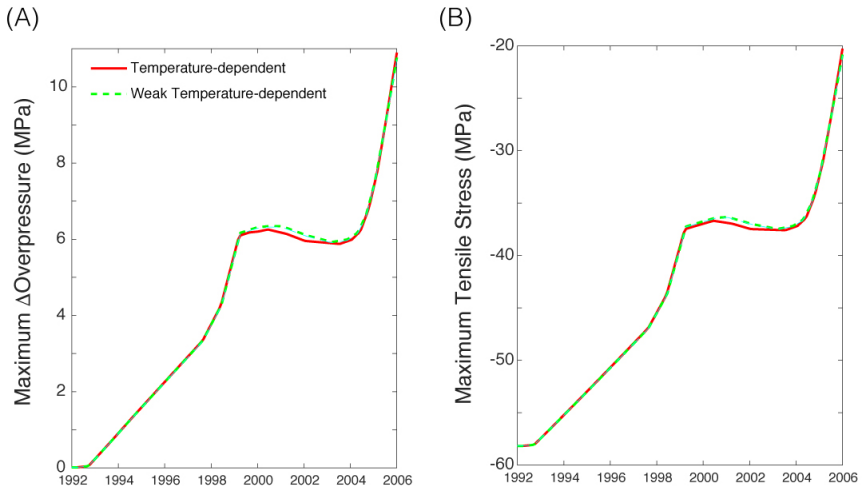

Figure S9. Comparison of the temperature-dependent model to the temperature-dependent model with pre-existing weaknesses. (A) The predicted maximum change in overpressure is very similar between the two models with the weak model (green dashed line) producing slightly higher maximum change in overpressure during the quiet period of 2001-2004. (B) Maximum tensile stress is predicted to be very similar between the temperature dependent (red line) and temperature-dependent pre-existing weakness (dashed green model).

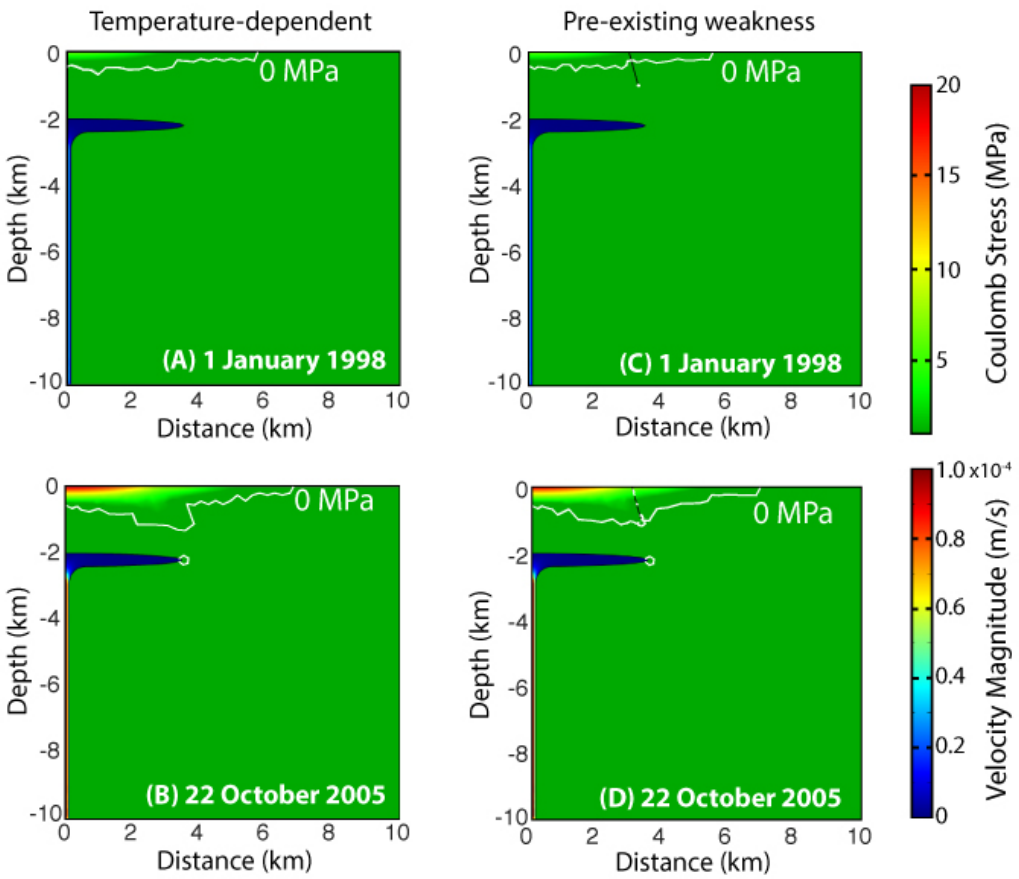

Figure S10. Modeled host-rock Coulomb stress and magma velocity magnitude. (A) Calculated Coulomb stress at 1 January 1998 just prior to the M_w5.0 earthquake on 11 January 1998 (Amelung *et al.*, 2000). White line is provided to highlight the 0 MPa contour. (B) Calculated Coulomb stress on 22 October 2005 just prior to the recorded M_w 5.4 at 2034 UTC and eruption at 2330 UTC. (C & D) Investigate the impact of a 20 m wide weak zone associated with a caldera ring fault.

A major caveat is the axisymmetric nature of the model that assumes a continuous ring fault. Future studies utilizing a fully 3D model would provide a better constraint on the dynamics of heterogeneities and preexisting weakness.

Table S1. Model Parameters

Parameter	Description	Value
A_D	Dorn parameter, Pa s	10^9
a	Vertical half-width, m	3500
b	Vertical half-height, m	200
C_P	Specific heat capacity, J kg^{-1} K^{-1}	1250
C	Cohesion, MPa	1
D_c	Depth to the top of magma reservoir, m	2000
E_A	Activation energy, J mol^{-1}	1e5
E_0	Initial Young's modulus, GPa	50
E_m	Minimum Young's modulus, GPa	5
f	Angle of internal friction, °	25
g	Gravitational acceleration, m s^{-2}	9.81
η_0	Host rock viscosity (Isoviscous model), Pa s	$5x10^{18}$
η_m	Effective magma viscosity, Pa s	$1x10^9$
θ	Angle of internal friction, °	25
k	Thermal conductivity, W m^{-1} K^{-1}	3
μ_0, μ_1	Fractional shear moduli	0.5
μ_f	Apparent friction coefficient	0.25
υ	Poisson's ratio	0.25
R_c	Conduit radius	100
R_g	Universal gas constant, J mol^{-1} K^{-1}	8.3114
ρ_m	Magma density, kg m^{-3}	2670
ρ_r	Host rock density, kg m^{-3}	2700
T_c	Temperature at the base of the conduit, °C	1200
T_m	Initial magma chamber temperature, °C	1130
T_{max}	Maximum Temperature, °C	1200
T_s	Surface temperature, °C	0
dT/dz	Geothermal gradient, K km^{-1}	30
z_{max}	Maximum model space depth, km	10

Table S2. Model Variables

Variable	Description
A_f	Fault area, m^2
β_m	Compressibility of the magma, Pa^{-1}
β_r	Compressibility of the host rock, Pa^{-1}
ΔCFF	Coulomb stress change, bars
ΔP	Pressure change, MPa
E_{td}	Temperature-dependent Young's modulus, Pa
ε	Strain
G	Shear modulus, Pa
η_{Td}	Temperature dependent viscosity, Pa s
θ	Angle with respect to horizontal, °
K	Bulk modulus, Pa
M_0	Seismic moment, dyne cm
M_w	Moment magnitude
r	Radial distance, polar coordinate system, m
S	Fault slip, m
σ	Stress, Pa
σ_n	Normal stress, Pa
σ_{ts}	Tensile stress in the r-z plane, Pa
σ_{ij}	Stress tensor, Einstein notation, Pa
$\Delta\sigma$	Change in normal stress, Coulomb stress calculation, bars
$\Delta\tau$	Change in shear stress, Coulomb stress calculation, bars
T	Temperature, K
t	Time
τ	Shear stress, Pa
u_x	Horizontal displacement, m
u_z	Vertical displacement, m
x	Horizontal distance, Cartesian coordinate system, m
z	Depth, positive up, m

Table S3. Numerical Experiment Results - Flux

Model Rheology	Flux (km^3/yr)		
	1992-1999	*2000-2003*	*2004 - 2005*
nTd elastic moduli, nTd viscosity (nTd1)	0.0092 to 0.023	-0.0018	0.0276 to 0.0460
nTd elastic moduli, Td viscosity (nTd2)	0.0095 to 0.03364	-0.0014625	0.02925 to 0.053625
Td elastic moduli, Td viscosity (Td)	0.011 to 0.03795	-0.0033	0.033 to 0.0605
Td elastic moduli, Td viscosity, Fault	0.011 to 0.03795	-0.0033	0.033 to 0.0605

Table S4. Numerical Experiment Results – Maximum change in overpressure

Model Rheology	Maximum Change in Overpressure (MPa)		
	1992-1999	*2000-2003*	*2004 - 2005*
nTd elastic moduli, nTd viscosity (nTd1)	18	18.9	27
nTd elastic moduli, Td viscosity (nTd2)	21.8	20.97	36.95
Td elastic moduli, Td viscosity (Td)	6.17	6.35	10.7
Td elastic moduli, Td viscosity, Fault	6.1	6.25	10.55

Table S5. Numerical Experiment Results – Maximum tensile stress

Model Rheology	Maximum Tensile Stress (MPa)*		
	1992-1999	*2000-2003*	*2004 - 2005*
nTd elastic moduli, nTd viscosity (nTd1)	39.75	43.2	88.5
nTd elastic moduli, Td viscosity (nTd2)	46.2	43.9	114
Td elastic moduli, Td viscosity (Td)	-38.0	-36.7	-20.8
Td elastic moduli, Td viscosity, Fault	-37.85	-36.4	-21.45

** Positive values indicate tension and negative values indicate compression.*

Table S6. Fault plane solutions for the 22 October 2005 earthquake as provided by the Global Central Moment Tensor (CMT) Catalog (Dziewonski *et al.*, 1981; Ekström *et al.*, 2012):

```
Date: 2005/10/22   Centroid Time: 20:34:47.6 GMT
Lat=  -1.00   Lon= -91.35
Depth= 12.0   Half duration= 1.3
Centroid time minus hypocenter time:  5.7
Moment Tensor: Expo=24  1.260 -0.989 -0.268 0.459 -1.510 0.080
Mw = 5.4    mb = 4.9    Ms = 0.0   Scalar Moment = 1.83e+24
Fault plane:  strike=285    dip=21   slip=49
Fault plane:  strike=148    dip=74   slip=104
```

References

Acocella, V. (2007), Understanding caldera structure and development; an overview of analog models compared to natural calderas, *Earth Science Reviews*, *85*, 125-160.

Acocella, V. (2010), Coupling volcanism and tectonics along divergent plate boundaries: Collapsed rifts from central Afar, Ethiopia, *Geol. Soc. Am. Bull.*, *122*(9-10), 1717-1728.

Amelung, F., S. Jonsson, H. Zebker, and P. Segall (2000), Widespread uplift and 'trapdoor' faulting on Galapagos volcanoes observed with radar interferometry, *Nature*, *407*(6807), 993-996.

Anderson, E. M. (1936), The dynamics of the formation of cone sheets, ring dykes, and cauldron subsidence, *Royal Society of Edinburgh Proceedings*, *56*(2), 128-163.

Anderson, E. M. (1951), *The dynamics of faulting and dyke formation with applications in Britain*, 2nd ed., Oliver and Boyd, London.

Chadwick, W. W., Jr., D. J. Geist, S. Jonsson, M. Poland, D. J. Johnson, and C. M. Meertens (2006), A volcano bursting at the seams: Inflation, faulting, and eruption at Sierra Negra volcano, Galapagos, *Geology*, *34*(12), 1025-1028.

de Silva, S. L., and P. M. Gregg (2014), Thermomechanical feedbacks in magmatic systems: Implications for growth, longevity, and evolution of large caldera-forming magma reservoirs and their supereruptions, *Journal of Volcanology and Geothermal Research*, *282*, 77-91.

Del Negro, C., G. Currenti, and D. Scandura (2009), Temperature-dependent viscoelastic modeling of ground deformation: Application to Etna volcano during the 1993-1997 inflation period, *Phys. Earth Planet. Int.*, *172*, 299-309.

Dziewonski, A. M., T.-A. Chou, and J. H. Woodhouse (1981), Determination of earthquake source parameters from waveform data for studies of global and regional seismicity, *J. Geophys. Res*, *86*, 2825-2852.

Ekström, G., M. Nettles, and A. M. Dziewonski (2012), The global CMT project 2004-2010: Centroid-moment tensors for 13,017 earthquakes, *Phys. Earth Planet. Int.*, *200-201*, 1-9.

Geist, D. J., K. S. Harpp, T. R. Naumann, M. Poland, W. W. Chadwick, M. Hall, and E. Rader (2008), The 2005 eruption of Sierra Negra volcano, Galapagos, Ecuador, *Bulletin of Volcanology*, *70*(6), 655-673.

Gerbault, M., F. Cappa, and R. Hassani (2012), Elasto-plastic and hydromechanical models of failure around an infinitely long magma chamber, *Geochemistry Geophysics Geosystems*, *13*.

Gregg, P. M., S. L. de Silva, E. B. Grosfils, and J. P. Parmigiani (2012), Catastrophic caldera-forming eruptions: Thermomechanics and implications for eruption triggering and maximum caldera dimensions on Earth, *Journal of Volcanology and Geothermal Research*, *241-242*, 1-12.

Gregg, P. M., S. L. de Silva, and E. B. Grosfils (2013), Thermomechanics of shallow magma chamber pressurization: Implications for the assessment of ground deformation data at active volcanoes, *Earth and Planetary Science Letters*, *384*, 100-108.

Grosfils, E. B. (2007), Magma reservoir failure on the terrestrial planets: Assessing the importance of gravitational loading in simple elastic models, *Journal of Volcanology and Geothermal Research*, *166*(2), 47-75.

Grosfils, E. B., P. J. McGovern, P. M. Gregg, G. A. Galgana, D. M. Hurwitz, S. M. Long, and S. Chestler (2015), Elastic models of magma reservoir mechanics: A key tool for understanding planetary volcanism, in *Volcanism and Tectonism Across the Inner Solar System*, edited by T. Platz, M. Massironi, P. Byrne and H. Hiesinger, pp. 139-158, Geological Society, London, Special Publications.

Hickey, J., and J. Gottsmann (2014), Benchmarking and developing numerical Finite Element models of volcanic deformation, *Journal of Volcanology and Geothermal Research*, *280*, 126-130.

Jonsson, S., H. Zebker, and F. Amelung (2005), On trapdoor faulting at Sierra Negra volcano, Galapagos, *Journal of Volcanology and Geothermal Research*, *144*(1-4), 59-71.

Le Mével, H., P. M. Gregg, and K. L. Feigl (2016), Magma injection into a long-lived reservoir to explain geodetically measured uplift: Application to the 2007–2014 unrest episode at Laguna del Maule volcanic field, Chile, *J. Geophys. Res*, *121*.

Lin, J., and R. S. Stein (2004), Stress triggering in thrust and subduction earthquakes and stress interaction between the southern San Andreas and nearby thrust and strike-slip faults, *Journal of Geophysical Research-Solid Earth*, *109*(B2).

Marti, J., A. Geyer, A. Folch, and J. Gottsmann (2008), A review on collapse caldera modelling, in *Caldera Volcanism: Analysis, Modelling and Response*, edited by J. Gottsmann and J. Marti, pp. 233-283.

Smith, R., P. R. Sammonds, and C. R. J. Kilburn (2009), Fracturing of volcanic systems: Experimental insights into pre-eruptive conditions, *Earth and Planetary Science Letters*, *280*, 211-219.

Toda, S., R. S. Stein, K. Richards-Dinger, and S. B. Bozkurt (2005), Forecasting the evolution of seismicity in southern California: Animations built on earthquake stress transfer, *Journal of Geophysical Research-Solid Earth*, *110*(B5).

Yun, S., P. Segall, and H. Zebker (2006), Constraints on magma chamber geometry at Sierra Negra Volcano, Galapagos Islands, based on InSAR observations, *Journal of Volcanology and Geothermal Research*, *150*(1-3), 232-243.